Compensation of Motion Artifacts in MRI via Graph-Based Optimization

Tung-Ying Lee Hong-Ren Su Shang-Hong Lai
Department of Computer Science
National Tsing Hua University
Hsinchu, Taiwan
d9562818@oz.nthu.edu.tw, a6880@ms25.hinet.net, lai@cs.nthu.edu.tw

Ti-chiun Chang
Siemens Corporate Research
Princeton, NJ, USA
ti-chiun.chang@siemens.com

Abstract

In two-dimensional Fourier transform magnetic resonance imaging (2DFT-MRI), patient/object motion during the image acquisition results in ghosting and blurring. These motion artifacts are commonly considered as a major limitation in the MRI community. To correct these artifacts without resorting to additional navigator echoes, most existing methods perform image quality measure to estimate motion; but they may easily fail when the motion is large. Viewed as a blind image restoration problem where the motion point spread function (PSF) is unknown, state-of-the-art restoration algorithms can not be easily applied because they cannot handle a complex PSF kernel that has the same size as the image. To overcome these challenges, we propose a novel approach that exploits the image structure to segment the kernel into several fragments. Based on this kernel representation, determining a kernel fragment can be formulated as a binary optimization problem, where each binary variable represents whether a segment in MR signals is corrupted by a certain motion or not. We establish a graphical model for these variables and estimate the kernel by minimizing an energy functional associated with the model. Experimental results show that the proposed method can provide satisfactory compensation of motion artifacts even when large motions are involved in the MR images.

1. Introduction

Patient or object motion during the magnetic resonance (MR) image acquisition can significantly degrade the image quality, resulting in diagnostically unacceptable artifacts such as ghosting and/or blurring. This has become a major limitation in MR examinations, especially when relatively large motion occurs. To address this issue, various approaches have been proposed. One way is to directly measure motion by employing additional navigator echoes (e.g., [1]); but some applications cannot afford the prolonged scan time or adopt the required special pulse sequences. Another approach exploits non-Cartesian trajectories in the frequency domain (usually referred to as k-space, where the MR signals are acquired) and is expected to be more robust to motion effect. However, it is generally understood that the conventional 2-D Fourier transform (2DFT) imaging (i.e., Cartesian trajectory) plays an important role for many applications and cannot be replaced. Some researchers [6] tried to estimate motion by attaching external markers to the imaging object. This method requires certain imaging assumptions which might not be practical in a clinical setting. Another approach, based on image quality measures to evaluate trial motion corrected image, is the focus of this research.

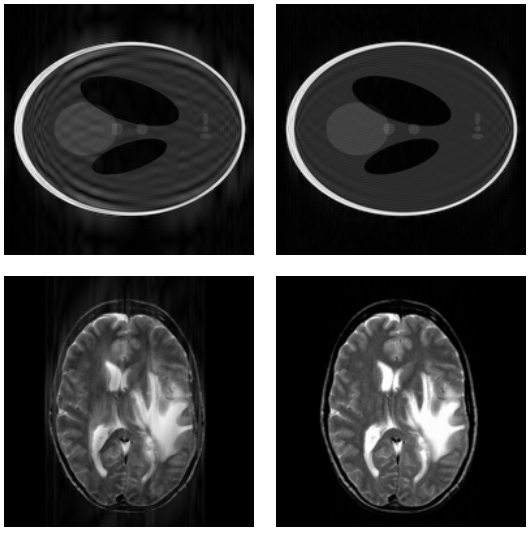

(a) (b)

Figure 1: (a) Images degraded by motion artifacts. (b) The corrected images by using the proposed motion compensation algorithm.

We first briefly describe MRI principles to better understand the cause of MRI motion artifacts. In MRI, time signals are mapped to the k-space (i.e., Fourier) coefficients of the target image. This scheme is known as spatial encoding. Generally, the x and y directions are, respectively, referred to as the frequency encoding and phase encoding directions. When k-space is filled with the

required signals that correspond to the desired field of view

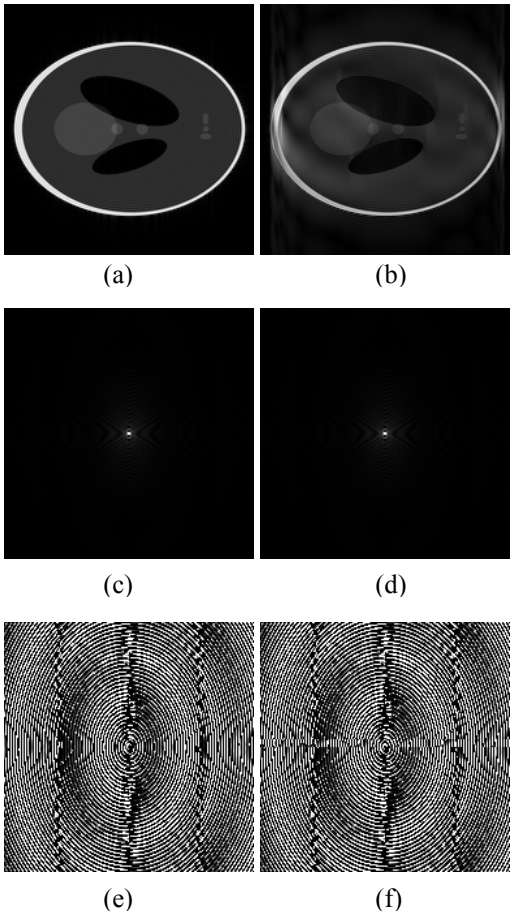

Figure 2: (a) The original image, (b) motion degraded image, (c) and (d) are, respectively, the magnitude of k-space data of (a) and (b), (e) and (f) are, respectively, the phase of k-space data of (a) and (b). In (f), several rows near the center are different from those in (e), because they are corrupted.

for the imaging object, a reconstruction algorithm—most often the inverse Fourier transform (IFT)—is used to generate an image.

Data acquisition is extremely fast in the frequency encoding direction, so motion can be ignored here. The time interval between two phase encoding (PE) lines is much longer. Therefore, object motion will take effect for different PE lines, incurring phase shift in k-space according to the Fourier transform property. The motion artifacts are the consequences of this phase shift. Removing motion artifacts is thus about recovering phase information in the frequency domain. Two motion corrupted examples are shown in Figure 1.

Based on this assumption, the image metric based methods (e.g., [5]) evaluate a set of trial motion for each PE line. The motion that yields the best measure is selected. Several methods have been applied to minimize certain image metrics and perform well for small motions. Aktinson et al. [2, 3] used the entropy criterion to determine the motions. Lin et al. [15] suggested to use normalized gradient squared (NGS) [4], where several clinical results are shown to be comparable to those from the navigator echo based techniques. More recently, to improve algorithm efficiency and robustness, they proposed the EXTRACT [14] method based on extrapolation of the k-space data and its correlation to prior corrected results.

The advantage of image metric based approach is that it does not require special pulse sequences. However, due to high dimensionality of the search space and the robustness issue of the image metrics, the correct minimizer is hard to obtain when the original MR signal is corrupted by large motions.

Viewed as a blind image restoration problem, where the motion point spread function (PSF) is unknown, the goal for motion correction is to estimate the corruption-free image and the motion PSF from the MR image directly. Similar restoration problems exist in different fields, such as radio astronomy, but the state-of-the-art deconvolution or deblurring methods cannot be applied here because our motion PSF kernel is a complex matrix whose size is as large as the target image.

In this paper, we propose a novel approach to address the issues described above. Our approach takes advantage of the special structure of the motion PSF kernel. We first detect dominant motion from the corrupted image. Then, we formulate the MRI motion estimation as a graph-based optimization problem. To be specific, the magnitude of the motion PSF kernel may contain many peaks, each corresponding to a motion vector. A large peak in the magnitude may represent artificial image structures due to ringing effect, with strong edges showing the most visible artifacts. Hence, we need to locate strong edges and the ringing counterparts from the image to estimate the peak locations in the PSF kernel. For each estimated motion vector, a binary variable is associated with a segment in k-space to denote if it is corrupted by this motion. The k-space partitioning segments are similar to those in [2]. We then combine all these binary variables in a graph, with which we associate an energy that is minimized to obtain the entire motion estimate. We perform several experiments and compare results with several image metric based methods. Experimental results show that the proposed method can provide satisfactory compensation for motion artifacts even when large motions are involved.

The rest of this paper is organized as follows: the formulation for the MRI motion correction problem is given in Section 2. The proposed novel motion artifact compensation algorithm is described in Section 3. Some experimental results are shown and compared with those

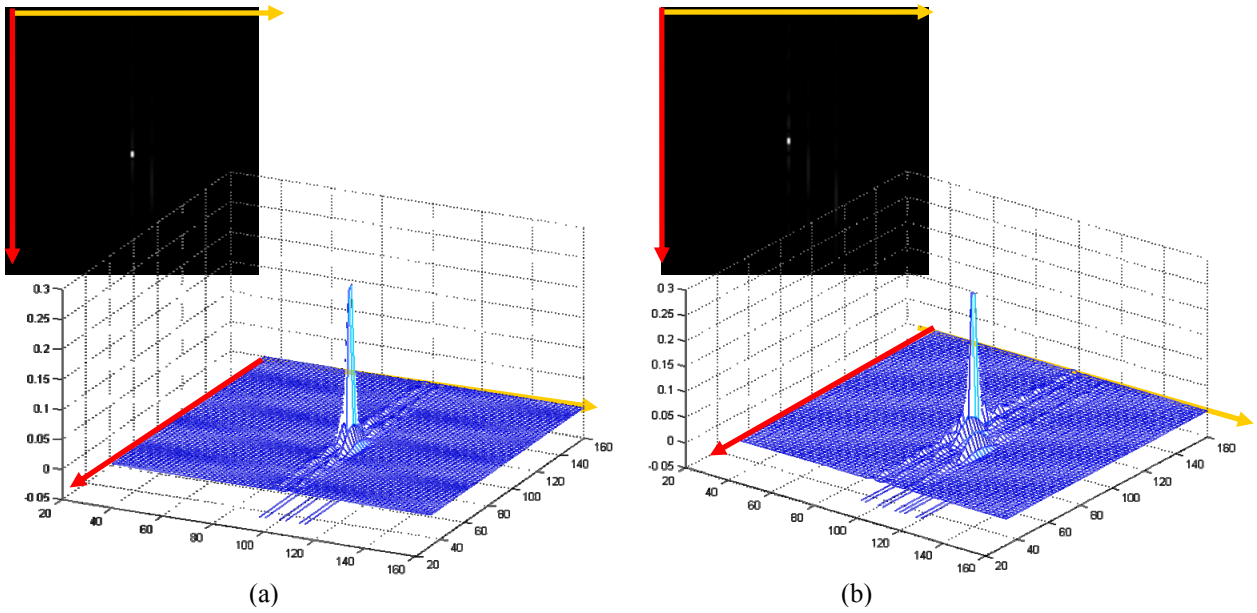

(a) (b)

Figure 3: The magnitude map of two kernels are shown. The kernel (a) has a single motion vector, and the kernel (b) has two different motion vectors. They are calculated by IFFT. The center means the (dx, dy) = (0, 0).

from existing methods in Section 4. Finally, Section 5 concludes this paper.

2. K-Space Data and Motion Artifact Kernel

2.1. Property of k-space data

It is known that a real signal/image exhibits Hermitian symmetry in the frequency domain, i.e., it is equal to its own conjugate transpose. Specifically, for a matrix **F**, we have $\mathbf{F} = \mathbf{F}^{\mathrm{H}}$, where the superscript H indicates the conjugate transpose. Although k-space data is complex due to MRI imaging principles, the object to be imaged is always real so that Hermitian symmetry could be expected, subject to all measurement imperfection.

2.2. Motion corruption process in spatial domain

When translational motion with shift (dx_n, dy_n) occurs and induces phase shift for the n-th phase encoding (PE) line, the overall motion transfer function **M** can be written as

$$\mathbf{M}\left(k_x,k_y\right)=\sum_{\forall n}\mathbf{M}^{n}_{dx_n,dy_n}\left(k_x,k_y\right), \tag{1}$$

where

$$\mathbf{M}^{n}_{dx_n,dy_n}\left(k_x,k_y\right)=\delta\left(0,k_y-n\right)\exp\left(-j2\pi\left(dx_n\cdot k_x+dy_n\cdot k_y\right)\right). \tag{2}$$

Here, k_x and k_y are, respectively, the indices for frequency-encoding and phase-encoding lines; $\delta(s, t)$ is the 2-d delta function that takes on the value 1 if $s = t = 0$, and 0 otherwise, and $\delta(t)$ is the 1-d delta function. Then, the corrupted k-space data **G** is the point-wise matrix multiplication (denoted by the symbol $\circ$) between the ideal k-space data **F** and the motion transfer function **M**

$$\mathbf{G}\left(k_x,k_y\right)=\mathbf{F}\left(k_x,k_y\right)\circ\mathbf{M}\left(k_x,k_y\right). \tag{3}$$

From Equation (3) and the convolution theorem, we know

$$FT^{-1}\left\{\mathbf{G}\right\}=FT^{-1}\left\{\mathbf{F}\right\}\otimes FT^{-1}\left\{\mathbf{M}\right\}, \tag{4}$$

where FT^{-1} and $\otimes$ denote, respectively, the inverse Fourier transform (IFT) and the 2D convolution. Thus, we can write the motion point spread function (PSF) kernel **k** as

$$\begin{aligned}\mathbf{k}(x,y)&=FT^{-1}\left\{\mathbf{M}\right\}\\&=\sum_{\forall n}\delta\left(x-dx_n,y-dy_n\right)\otimes\left[\exp\left(-j2\pi y\cdot n\right)\delta(x)\right]\end{aligned} \tag{5}$$

where the constant scaling factor in the Fourier transform pair is ignored. We see that the magnitude of the PSF kernel is constant along the y direction, if only one motion (dx_n, dy_n) results in phase shift at the n-th PE line and the other PE lines are uncorrupted. If the entire k-space resulting from this single motion is known, we will be able to see a peak at (dx_n, dy_n) in the PSF. Figure 3(a) illustrates an

example kernel when a single motion leads to 8 corrupted PE lines.

3. Proposed Motion Correction Algorithm

The proposed algorithm can be divided into three parts. First, we detect and estimate dominant motion, and then we create a graphical model for each estimated motion vector. Finally, the corrupted segments for each dominant motion are restored by minimizing the energy associated with the graphical model. The following subsections give detailed descriptions of our algorithm.

3.1. Estimation of motion vectors

To better detect object boundary structures in the motion corrupted image, we first perform Canny edge detection (CED) [8]. This will allow us to create desirable templates to perform normalized cross correlation (NCC), which we will describe shortly. Then we calculate the gradient map. The edge fragments from CED with high gradient magnitude are regarded as strong structures, which, together with their neighboring pixels, are collected to form a set of templates. These templates are not necessarily rectangle, and may be arbitrary-shaped.

To estimate motion vector, we apply the template matching approach by NCC, defined as

$$NCC(x,y)=\frac{\sum_{i,j\in T}\left(T(i,j)-\bar{T}\right)\left(I(x+i,y+j)-\bar{I}\right)}{\sqrt{\sum_{i,j\in T}\left(T(i,j)-\bar{T}\right)^2}\sqrt{\sum_{i,j\in T}\left(I(x+i,x+j)-\bar{I}\right)^2}}, \tag{6}$$

where $\bar{T}$ is the mean intensity of the template T; and $\bar{I}$ is the mean intensity of the image with (x, y) coincided with the center of T. NCC is performed only for low gradient magnitude map where strong structures are removed. This is because we assume that the true structures have stronger gradients than those of ghosting structures. According to NCC, the distances between the template center and the location with high response yield candidates for motion vectors. Finally, a voting array containing all motion vectors is used to collect responses from different NCC matching results.

3.2. Graphical model construction and optimization

For each motion vector (dx, dy), we must determine whether the segment is corrupted or not. We make use of the image quality metric and the conjugate symmetric property for the motion-free k-space data to create a graphical model. In this work, the normalized gradient squared (NGS) [5] is used as the image quality metric. A greater NGS value for an input image I, computed according to

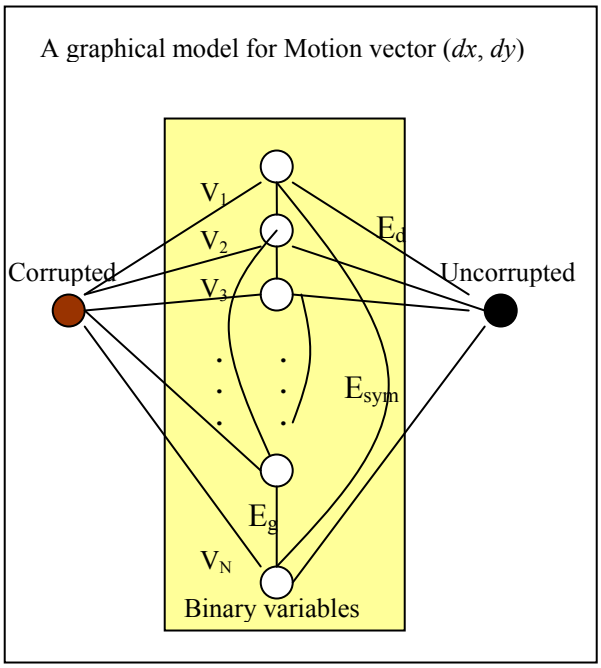

Figure 4: A graphical model for a dominant motion vector (dx, dy) contains N binary nodes, and three types of energies are shown in the figure.

$$NGS(I)=\frac{\sum_{x,y}\|\nabla I\|^2}{\left(\sum_{x,y}\|\nabla I\|\right)^2}, \tag{7}$$

implies better image quality. The graphical model for determining whether a segment is corrupted due to motion is depicted in Figure 4. Here, the number of binary nodes is the same as the number of PE lines N. The i-th binary variable V_i models whether the i-th PE line is corrupted or not. Hence, the problem is transformed into a labeling problem. The energy E for this labeling problem is composed of three terms with weighting coefficients α and γ:

$$E=\sum_i E_d(V_i)+\gamma\sum_{|i-j|=1}E_g(V_i,V_j)+\alpha\sum_{i+j=2N}E_{sym}(V_i,V_j). \tag{8}$$

We elaborate each term below. First, $E_d(V_i)$ is defined by NGS according to Equation (7). It can be interpreted as a data fidelity term in our graphical model, as it evaluates the goodness of the trial solution (i.e., $E_d(V_i=1)$), compared to the that of the input image $E_d(V_i=0)$. In our notation, $E_d(V_i=1)$ is the NGS value of the image when the motion (dx, dy) is corrected at the i-th row, i.e.,

$$\mathbf{S}^{i}_{-dx,-dy} = \mathbf{M}^{i}_{-dx,-dy}\left(k_x, k_y\right) + \sum_{n \neq i} \mathbf{M}^{n}_{0,0}\left(k_x, k_y\right)$$

$$E_d\left(V_i = 1\right) := -NGS\left(\left|FT^{-1}\left\{\mathbf{F} \circ \mathbf{S}^{i}_{-dx,-dy}\right\}\right|\right). \quad (9)$$

The term $E_g(V_i, V_j)$ penalizes the case when two adjacent PE lines are not simultaneously motion-compensated. This embodies the fact that adjacent PE lines should undergo similar motion conditions. Explicitly, we define $E_g(V_i=1,V_j=1)$ as

$$E_g\left(V_i = 1, V_j = 1\right) := -NGS\left(\left|FT^{-1}\left\{\mathbf{G} \circ \mathbf{S}^{i}_{-dx,-dy} \circ \mathbf{S}^{j}_{-dx,-dy}\right\}\right|\right) - E_d\left(V_i = 1\right) - E_d\left(V_j = 1\right). \quad (10)$$

If two adjacent rows have different labels, we simply assign a constant to $E_g(V_i,V_j)$:

$$E_g\left(V_i = 0, V_j = 1\right) := \beta$$
$$E_g\left(V_i = 1, V_j = 0\right) := \beta$$
$$E_g\left(V_i = 0, V_j = 0\right) := 0.$$

Finally, $E_{sym}(V_i, V_j)$ is a regularization term that enforces conjugate symmetry of k-space data given the label of i-th and j-th PE lines. If V_i=1 or V_j=1, it means that the motion (dx, dy) is applied to the corresponding row. Then, the magnitude **D** of the difference of the k-space data and its Hermitian transpose is calculated. $E_{sym}(V_i, V_j)$ is defined by the Frobenius norm of this matrix **D**:

$$E_{sym}\left(V_i = 1, V_j = 1\right) := \left\|\mathbf{G} \circ \mathbf{S}^{i}_{-dx,-dy} - \left(\mathbf{G} \circ \mathbf{S}^{j}_{-dx,-dy}\right)^{H}\right\|_F^2$$
$$E_{sym}\left(V_i = 1, V_j = 0\right) := \left\|\mathbf{G} \circ \mathbf{S}^{i}_{-dx,-dy} - \mathbf{G}^{H}\right\|_F^2$$
$$E_{sym}\left(V_i = 1, V_j = 0\right) := \left\|\mathbf{G} - \left(\mathbf{G} \circ \mathbf{S}^{j}_{-dx,-dy}\right)^{H}\right\|_F^2$$
$$E_{sym}\left(V_i = 0, V_j = 0\right) := \left\|\mathbf{G} - \mathbf{G}^{H}\right\|_F^2. \quad (11)$$

After constructing the graphical model, we apply the iterated conditional modes (ICM) algorithm [7] to cut the edges of the graph. For the nodes classified as corrupted, the inverse motions are applied to the k-space data. The parameters of the graph are updated and all variables are classified again until no variables are labeled corrupted.

3.3. Overall algorithm

The overall algorithm is summarized here:

1. Perform edge detection and calculate the gradient magnitude map.
2. Select the regions containing edge fragments with high gradient magnitude as templates, T_i, i=1,..,n. In practice, the dilation operator can be applied on the edge fragment.
3. Create low-gradient-magnitude map **L** by removing the regions with high gradient magnitudes. For example, a threshold, above which the gradients are removed, can be used.
4. For each T_i, perform NCC to find the displacements with high responses. Select candidate motion vectors $\{(dx_i,dy_i)\}$ from the displacement vectors.
5. For each candidate vector (dx_i,dy_i), create a graphical model and calculate all related terms by using Equation (7-11).
6. Perform iterated conditional modes (ICM) algorithm to determine the corrupted segments. Compensate the corresponding segments with estimated motion vectors.
7. Re calculate the energy on the current graphical model and repeat step 6. If there is no change, perform step 6 on the other graphical models.

4. Experimental Results

To evaluate the proposed algorithm, we collect several sets of data. The first one is a bottle phantom with true k-space data obtained from a MR imager (**MR**). We also use the Shepp and Logan head phantom (**SL**) and brain MR images [18] to generate k-space data for testing.

We simulate motion corrupted data by using several large motions on the k-space data. Each dataset contains several large motions.

If true motion displacement is not integer-valued, in most cases, our method can find the closest integer motion vectors to compensate the motion artifacts. Some examples are shown in Figure 6. The motions in Figure 6 are similar to those in Figure 5, but the motion vectors are not integer motions.

For quantitative analysis, we also calculate the NGS values for all our results. The NGS has been used for assessing the quality of the corrected MR images. The comparison is shown in Table 1. Compared with the input corrupted data, the average NGS gain of our method is 28.85%. This is significantly better than the negative performance -24.73% by using EXTRACT, and still 2 times better than the gain 14.55% by using min-NGS method. Table 2 shows similar comparison on the corrected brain MR images.

We compare our method with the image-metric based

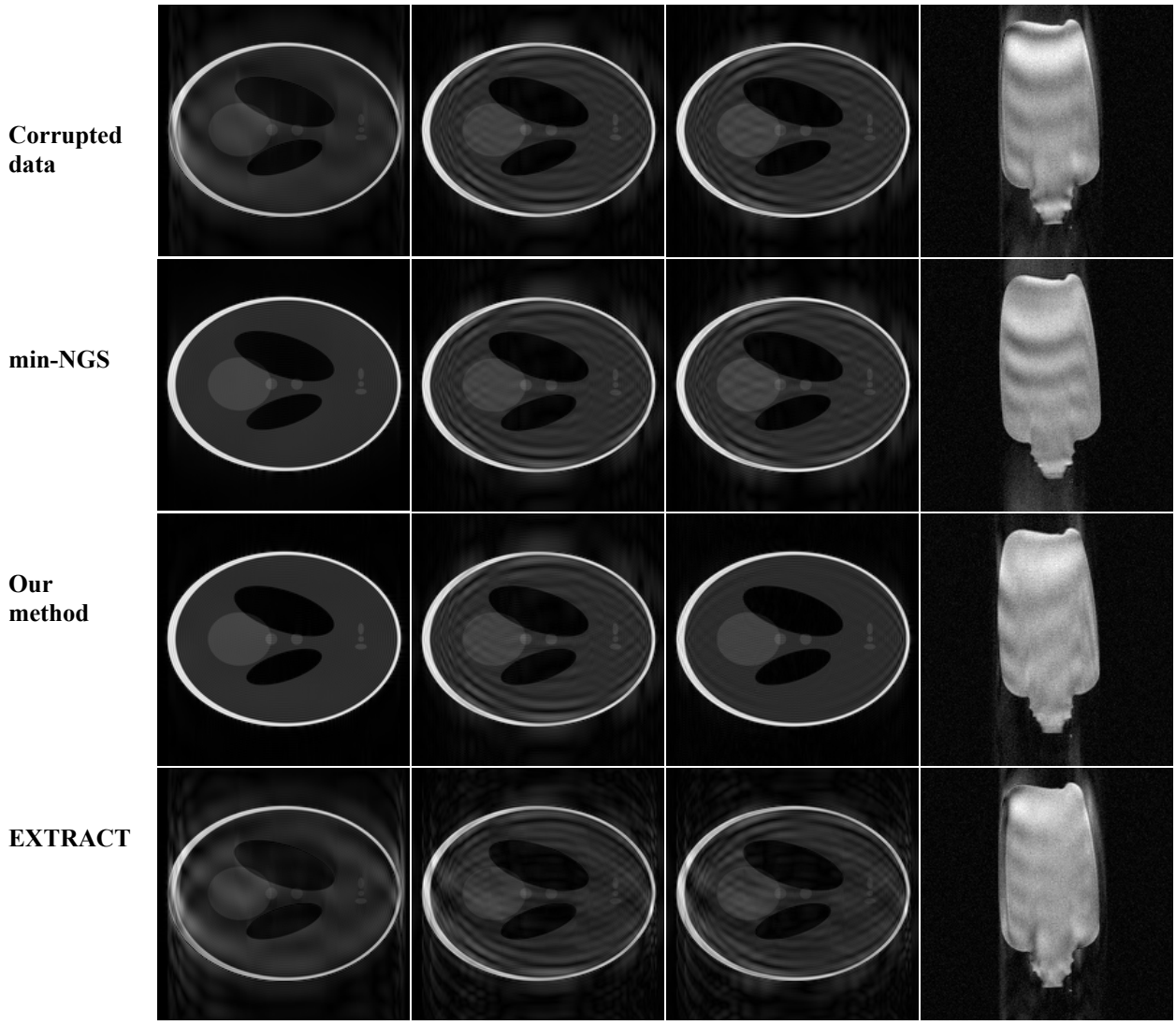

(a) SL1 (b) SL2 (c) SL 3 (d) MR 1

Figure 5: Experimental results on Shepp and Logan phantom data (a-c) and MR scanned phantom (d).

method. Its metric is the NGS, and we use BFGS [10-13] method with a cubic line search as the optimization procedure because the size of the metric map is hard to decide and it performs well in most situations. In Figure 6 (a), the min-NGS method compensates most of the motion artifacts except that there exists some ghosting in the left part of phantom.

There are some difficult cases in our experiments. For example, both the NGS method and our method cannot provide satisfactory motion correction results in Figure 5(b). Our method does not perform well in this case because the dominant motion detection procedure failed to detect the true motion in the first step.

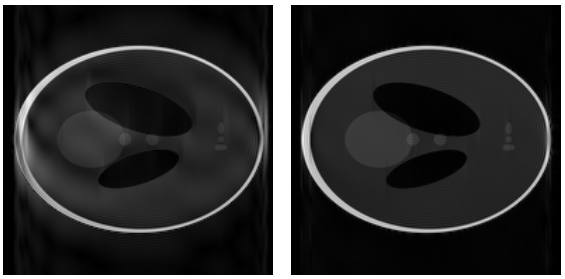

(a) (b)

Figure 6: (a) A motion corrupted image with non-integer motion which are similar those to Figure 5(a), and (b) the corrected result by using our method.

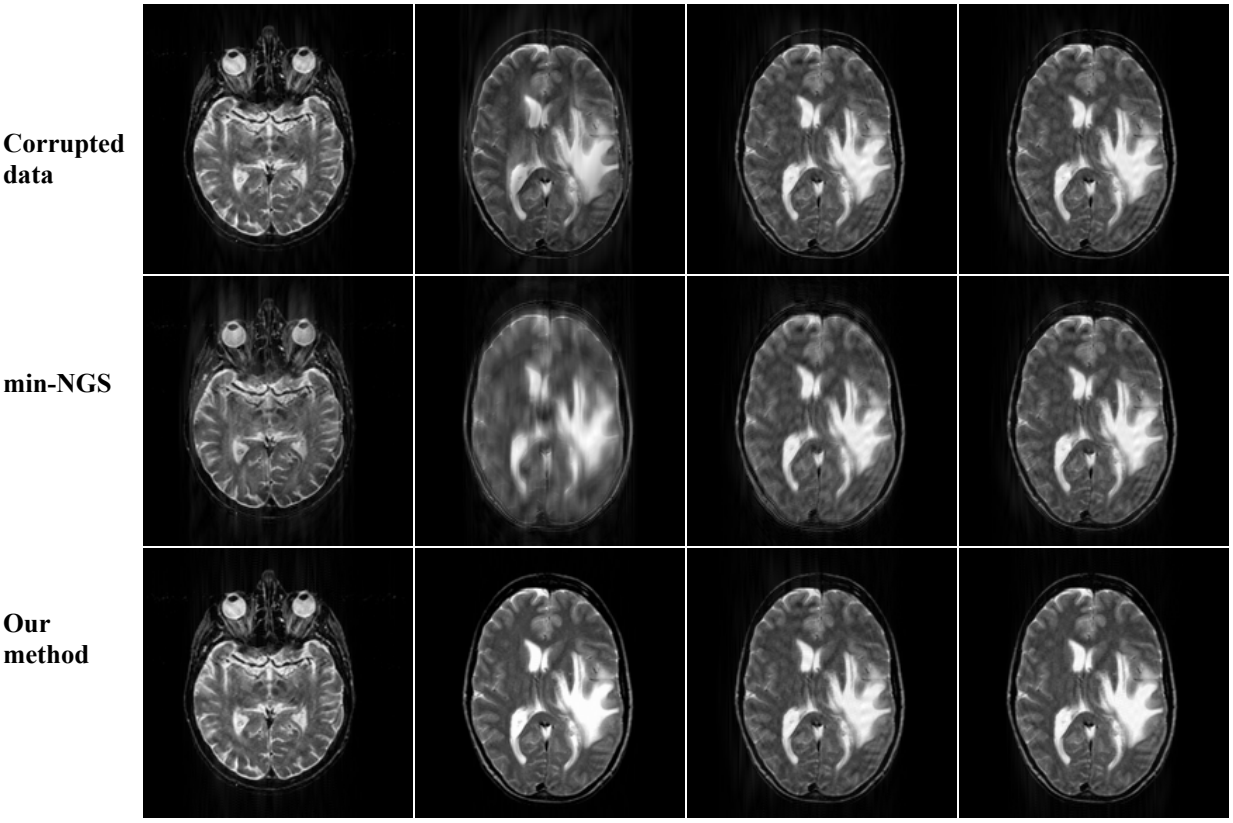

(a) Brain 1 (b) Brain 2 (c) Brain 3 (d) Brain 4

Figure 7: Experimental results on Brain MR images.

Table 1: The NGS[1] gain on SL.

Dataset	Corrupted data	Our method	min-NGS	EXTRACT
SL1	2.2370e-4	3.1295e-4	3.1764e-4	1.7995e-4
SL2	1.7733e-4	1.7782e-4	1.7914e-4	1.2861e-4
SL3	1.7715e-4	2.5929e-4	1.7830e-4	1.2902e-4
Mean gain	0%	28.85%	14.55%	-24.73%

Table 2: The NGS gain on MR and Brain MR.

Dataset	Motion-corrupted	Our method	min-NGS
MR1	8.9624e-5	1.1338e-4	1.1996e-4
MR2	1.1748e-4	1.2571e-4	1.2557e-4
MR3	1.1941e-4	1.5839e-4	1.2831e-4
Brain1	1.0214e-4	1.0805e-4	1.0869e-4
Brain2	9.4636e-5	1.1949e-4	1.0115e-4
Brain3	1.0442e-4	1.0667e-4	1.0507e-4
Brain4	1.0473e-4	1.1224e-4	1.0514e-4
Mean gain	0%	15.36%	8.93%

[1] In order to avoid the effect of shift, these NGS values in our tables are calculated circularly.

5. Conclusion

We constructed a graphical model and associated with it an energy functional that consists of an image quality metric, and motion smooth and data symmetry constraints. Based on this model, motion correction is converted to a labeling problem, where ICM is used to minimize the energy functional. Binary variables are used to represent whether motion occurs in the corresponding k-space segments. These variables have strong dependency because motion is better correlated within a very short time period. Our graphical model is built to explore this correlation. Previous image-metric based methods failed to exploit this dependency in the MRI motion compensation process. Because our algorithm takes this into account, our results are more robust to incorrect motion estimate. We compared the proposed motion compensation algorithm with NGS and EXTRACT methods in the experiments. The experimental results showed the proposed algorithm performs well in most cases even when large motions are involved in the motion artifacts.

Finally, we note that other Markov random field (MRF) minimization methods can also be used to solve our energy functional, such as TRW-S [17]. A comparative study [16]

has shown different minimization methods may yield different results. As a future work, we would like to combine the graphical models for different motion vectors into a whole graphical model in order to better describe the correlation between different motion vectors.

Acknowledgements

The authors would like to thank Dr. Ronald Ouwekerk for his matlab code to generate Shepp and Logan head phantom.

References

[1] R. L. Ehman and J. P. Felmlee. Adaptive technique for high-definition mr imaging of moving structures, *Radiology*. vol. 173, no. 1, pp. 255-263, October 1989.

[2] D. Atkinson, D. L. G. Hill, P. N. R. Stoyle, P. E. Summers, and S. F. Keevil. Automatic correction of motion artifacts in magnetic resonance images using an entropy focus criterion. *IEEE Transactions on Medical Imaging*, vol. 16, no. 6, pp. 903-910, 1997.

[3] D. Atkinson, D. L. Hill, P. N. Stoyle, P. E. Summers, S. Clare, R. Bowtell, and S. F. Keevil. Automatic compensation of motion artifacts in MRI. *Magnetic Resonance in Medicine*, vol. 41, no. 1, pp. 163-170, January 1999.

[4] A. Manduca, K. P. McGee, E. B. Welch, J. P. Felmlee, R. C. Grimm, and R. L. Ehman. Autocorrection in mr imaging: adaptive motion correction without navigator echoes. *Radiology*, vol. 215, no. 3, pp. 904-909, June 2000.

[5] K. P. Mcgee, A. Manduca, J. P. Felmlee, S. J. Riederer, and R. L. Ehman. Image metric-based correction (autocorrection) of motion effects: Analysis of image metrics. *Journal of Magnetic Resonance Imaging*, vol. 11, no. 2, pp. 174-181, 2000.

[6] A. S. Fahmy, B. Tawfik, and Y. M. Kadah. Robust estimation of planar rigid body motion in magnetic resonance imaging. *Proc. International Conference on Image Processing*, vol. 2, 2000, pp. 487-490 vol.2.

[7] J. Besag. On the statistical analysis of dirty pictures. *Journal of the Royal Statistical Society. Series B*, vol. 48, no. 3, pp. 259-302, 1986.

[8] J. Canny. Computational Approach To Edge Detection. *IEEE Trans. Pattern Analysis and Machine Intelligence*, 8:679-714, 1986.

[9] R. Van De Walle, H. H. Barrett, K. J. Myers, M. I. Aitbach, B. Desplanques, A. F. Gmitro, J. Cornelis, and I. Lemahieu, Reconstruction of MR images from data acquired on a general nonregular grid by pseudoinverse calculation. *IEEE Transactions on Medical Imaging*, vol. 19, no. 12, pp. 1160-1167, 2000.

[10] C. G. Broyden. The convergence of a class of double-rank minimization algorithms. *Journal Inst. Math. Applic*., vol. 6, pp. 76-90, 1970.

[11] R. Fletcher. A new approach to variable metric algorithms. Computer Journal, vol. 13, pp. 317-322, 1970.

[12] D. Goldfarb. A family of variable metric updates derived by variational means. *Mathematics of Computing*. vol. 24, pp. 23-26, 1970.

[13] D. F. Shanno. Conditioning of Quasi-Newton methods for function minimization. *Mathematics of Computing*, vol. 24, pp. 647-656, 1970.

[14] W. Lin, and H. K. Song. Extrapolation and correlation (EXTRACT): a new method for motion compensation in MRI, to appear in *IEEE Transactions on Medical Imaging*. (Paper available online from IEEE Xplore)

[15] W. Lin and H.K. Song. Improved optimization strategies for autofocusing motion compensation in MRI via the analysis of image metric maps. In *Magn. Reson. Imag.* 24(2006):751-760.

[16] R. Szeliski, R. Zabih, D. Scharstein, O. Veksler, V. Kolmogorov, A. Agarwala, M. Tappen, and C. Rother. A Comparative study of energy minimization methods for Markov random fields with smoothness-based priors. *IEEE Trans. on Pattern Analysis and Machine Intelligence,* vol. 30, no. 6, pp. 1068-1080, 2008.

[17] V. Kolmogorov. Convergent tree-reweighted message passing for energy minimization. *IEEE Trans. on Pattern Analysis and Machine Intelligence*, vol. 28, no. 10, 2006.

[18] Keith A. Johnson and A. Becker. The Whole Brain Atlas. http://www.med.harvard.edu/AANLIB/home.html